Label-free protein analysis using liquid chromatography with gravimetric detection

Tadas Kartanas,[†] Aviad Levin,[†] Zenon Toprakcioglu,[†] Tom Scheidt,[†] Tuuli A. Hakala,[†] Jerome Charmet,[†,‡] and Tuomas P. J. Knowles[*,†,¶]

[†]*Centre for Misfolding Diseases, Yusuf Hamied Department of Chemistry, University of Cambridge, Lensfield Road, Cambridge CB2 1EW, UK*

[‡]*WMG, University of Warwick, Coventry, CV4 7AL, United Kingdom*

[¶]*Cavendish Laboratory, University of Cambridge, Cambridge CB3 0FE, UK*

E-mail: tpjk2@cam.ac.uk

Abstract

The detection and analysis of proteins in a label-free manner under native solution conditions is an increasingly important objective in analytical bioscience platform development. Common approaches to detect native proteins in solution often require specific labels to enhance sensitivity. Dry mass sensing approaches, by contrast, using mechanical resonators, can operate in a label-free manner and offer attractive sensitivity. However, such approaches typically suffer from a lack of analyte selectivity as the interface between standard protein separation techniques and micro-resonator platforms is often constrained by qualitative mechanical sensor performance in the liquid phase. Here, we describe a strategy that overcomes this limitation by coupling liquid chromatography (LC) with a quartz crystal microbalance (QCM) platform by using a microfluidic spray dryer. We explore a strategy which allows first to separate a protein

mixture in a physiological buffer solution using size exclusion chromatography, allowing specific protein fractions to be selected, desalted and subsequently spray-dried onto the QCM for absolute mass analysis. By establishing a continuous flow interface between the chromatography column and the spray device via a flow splitter, simultaneous protein mass detection and sample fractionation is achieved, with sensitivity down to a 100 µg/mL limit of detection. This approach for quantitative label-free protein mixture analysis offers the potential for detection of protein species under physiological conditions.

Introduction

Quantitative label-free biomolecular detection is an integral part of basic applied research in fields ranging from physics to chemistry and medicine, with a wide range of industry related applications.[1–7] The requirement to detect a variety of biomolecules in a scalable and cost effective manner can, however, limit traditional diagnostic techniques as these require additional characterisation steps.[8,9] Recent development of sensitive and accurate label-free protein detection tools combined with micro-technology platforms open up numerous possibilities to address this challenge, while also allowing to explore the fundamental principles related to native protein interactions in solution.[6,10–13]

Mechanical mass detection is a conceptually simple but robust technique that yields an absolute gravimetric measure of physical objects attached to the detector surface. In dynamic mode, the downward resonant frequency shifts resulting from analytes binding to a mechanical resonator give a direct measurement of the added mass. Acoustic resonators can be mass produced[8] and integrated into low cost platforms offering unprecedented limits of detections, as low as 7 zeptograms.[14,15] However, such gravimetric sensors are usually not ideal for protein detection purposes due to their reduced sensitivity in liquids, as well as the requirement for specific surface functionalisation enabling selective protein detection.[16–20] One of the most commercially successful sensor devices - quartz crystal microbalance (QCM)

- is an established mass analysis approach for the detection of a range of molecules with sub-nanogram resolution.[21–23] Even though such transducers can be operated in liquid,[24–26] and have been integrated with microfluidic flow cells[27,28] or sensors,[29–31] the interpretation of liquid-based measurements remain challenging.[17,32] To explore the full capability of acoustic sensor performance, we have recently demonstrated the use of dry mass sensing using a microfluidic spray-drying approach in combination with QCM sensing.[33–35] This platform has allowed the detection of biomolecules in the gas phase, thus overcoming challenges present if the measurement is performed in a liquid environment, such as a decrease in the quality factor of the sensor and the viscous drag. However, this approach is not suitable for the characterisation of biomolecular mixtures, offering overall mass measurement with little selectivity or specificity to different molecular species found in solution.

Protein separation is necessary for scalable label-free detection platforms extending beyond the detection of a single analyte is solution.[36,37] There are a wide range of established protein separation techniques, such as capillary electrophoresis,[38] liquid chromatography (LC)[39] and free flow-electrophoresis.[40] In particular, LC used in biological research relies on the interaction between a stationary phase and the analyte within the mobile phase. The most commonly used LC methods include size-exclusion,[41] reversed phase,[42] ion-exchange[43] and affinity chromatography.[44]

Here, we present a general strategy to couple dry mass sensing with protein upstream separation techniques using microfluidic spray-drying. We thus couple a size exclusion column with QCM detection through a microfluidic spray nozzle for real-time, continuous mass measurement (Figure 1). The spray nozzle nebulises the liquid into micron-sized drops,[33,34,45] thus, enhancing the liquid evaporation rate which is essential for a continuous surface spray drying. To perform selective protein sensing within conventional physiological buffers, we incorporate a desalting step[46] following protein separation and demonstrate a concentration sensitive dry mass detection of a label-free protein in a complex mixture. The presented platform further capitalises on applying multidimensional protein characterisation using mi-

crofluidic post-column analysis, as has recently been demonstrated,[47] extending such techniques for the detection of label-free proteins in complex solution conditions. Such a system may prove particularly useful for measuring sample concentration in cases when UV molecular absorption is weak or where changes in molecular conformational affect light absorbance, thus making accurate quantitation challenging using conventional methodologies.

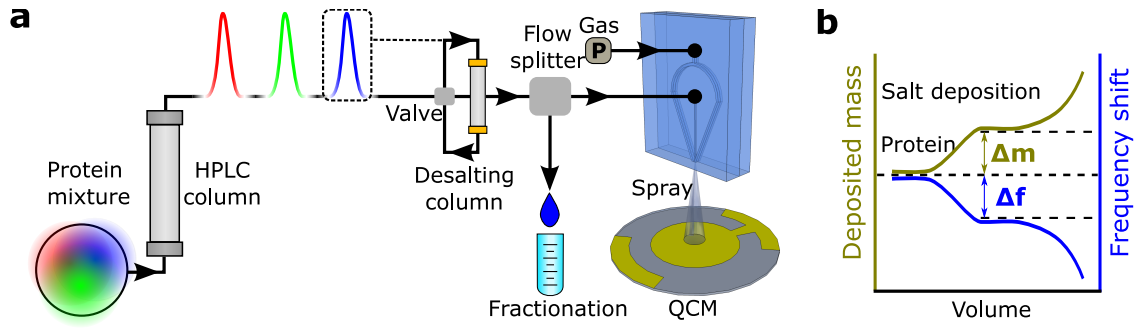

Figure 1: Integration of a liquid chromatography purification column with gravimetric QCM detection. (a) The protein mixture was separated on the LC column and a specific fraction was selected and injected into a protein desalting column using a standard injection valve. The desalted protein fraction then flows via a splitter to a microfluidic nebuliser continuously, spray-drying the solution on to a QCM. (b) The QCM sensor records a decreasing resonant frequency indicating continuous mass deposition on the surface. The desalted protein fraction causes a sharp frequency decrease followed by a delayed buffer salt deposition, enabling selective label-free purely gravimetric protein mass detection.

Experimental methods

In brief, we have combined liquid chromatography (LC) with a QCM via a microfluidic nebuliser (Figure 1). A flow splitter was used to combine the high flow from the liquid chromatography with the microfluidic spray, which operates at a flow rate that is an order of magnitude lower. The passive flow splitter device enabled simultaneous sample fractionation and gravimetric analysis. To detect the mass of proteins after the separation step, a standard desalting column in sequence to the main LC column was incorporated, thus allowing for selective concentration sensitive protein detection.

Device fabrication

Microfluidic devices were fabricated using a standard polydimethylsiloxane (PDMS) soft lithography approach.[48] The spray device contains two inlets for the nebulising nitrogen gas and the liquid sample, as shown in Figure 2. The liquid channel length is L_{in}=8.1 mm with a cross section of 25×20 µm^2, while the gas channel has a length of L_{gas}=8.4 mm, with a cross section of 100×100 µm^2. The 3-D junction was prepared by plasma bonding two PDMS complementary replicas using a previously established method,[34,49,50] to allow for the emerging liquid to be surrounded by a gas flow to transport the fluid outside the nozzle through a jet without wetting the PDMS surface. The device gas inlet was then connected to a compressed nitrogen cylinder with a pressure regulator typically set to 3 bar and the liquid inlet was connected to an outlet of a flow splitter.

Liquid chromatography sample separation and desalting

To demonstrate the functionality of this method, a mixture of three proteins from a standard kit (GE Healthcare, 28-4038-42) was prepared, containing bovine thyroglobulin (670 kDa), rabbit aldolase (158 kDa) and chicken ovalbumin (43 kDa). The proteins were diluted in 1XPBS buffer (pH 7.3) to reach a total volume of 40 µL. The concentration of thyroglobulin was varied between 0.5-2 mg/mL while the concentration of aldolase and ovalbumin was fixed to 1 mg/ml.

A 1XPBS, pH 7.3, buffer was also used for the sample elution through a Superdex 200 Increase 3.2/300 column (GE Healthcare, UK). The LC flow was varied around a typical value of 25 µL/min and controlled by an ÄKTA Pure System (GE Healthcare, UK). We monitored the eluting sample absorption at 280 nm with a 10 mm path length absorption monitor U9-M (GE Healthcare, UK) and the solution conductivity was measured with a conductivity monitor C9 (GE Healthcare, UK). Protein desalting was carried out with a water filled HiTrap desalting column (GE Healthcare, 17-1408-01) connected through a standard injection valve with the main flow path. The protein to be desalted was selectively guided

into the desalting column, and following this, the flow was subsequently connected to the microfluidic flow splitter.

Flow splitter

A microfluidic flow splitter comprising of a Y split (P-512, IDEX Health & Science) with carefully pre-cut polyether ether ketone (PEEK) capillaries (IDEX Health & Science) and a flow sensor MF2 (Elveflow) was built, splitting only a fraction of the flow coming from chromatographic separation into the microfluidic spray device (Figure 2b). The flow splitter output is made of a capillary with length L_f=32.4 cm and 67.8 µm ID giving the hydraulic resistance R_2=5.57 · 10^{14} Pa·s/m^3. The capillary connecting the splitter to the spray is of length L_s=10 cm and 125 µm ID, giving a hydraulic resistance of 1.5 · 10^{13} Pa·s/m^3. The on-chip resistance of the narrow liquid channel can be estimated to be 8.8 · 10^{14} Pa·s/m^3, thus dominating the total hydraulic resistance R_1 of the liquid flow path to the spray.

Assuming the pressure at the splitter is P_T, the total flow Q_{LC} is distributed between the spray nozzle (pressure P_S, flow Q_1 and resistance R_1) and the flow splitter outlet (atmospheric pressure P_0, flow Q_2 and resistance R_2). By flow conservation at the splitter:

$$Q_{LC} = Q_1 + Q_2 = \frac{P_T - P_S}{R_1} + \frac{P_T - P_0}{R_2} \tag{1}$$

Then the liquid flow to the spray can be expressed as:

$$Q_1 = \frac{P_T - P_S}{R_1} = \frac{R_2}{R_1 + R_2} Q_{LC} - \frac{P_S}{R_1 + R_2} = mQ_{LC} + c \tag{2}$$

indicating a linear relationship between Q_1 and Q_{LC}. Using the values stated above we estimate the gradient and the intercept to be m=$R_2/(R_1 + R_2)$ = 0.38 and c=$-P_S/(R_1 + R_2)$ = - 740 µL/h, respectively.

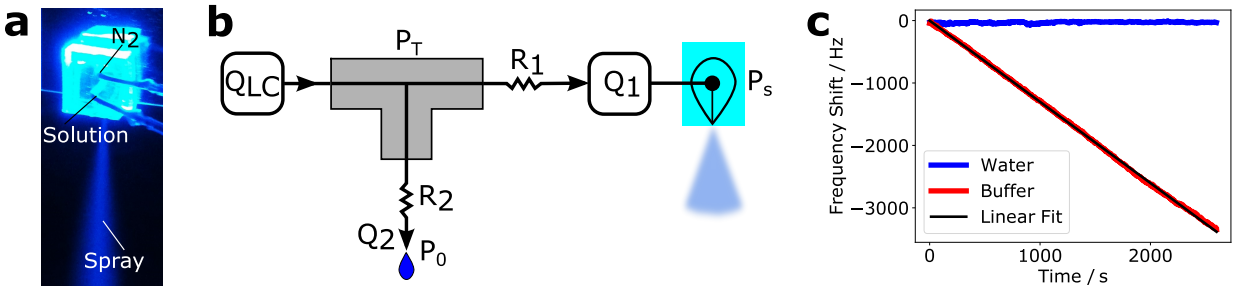

Figure 2: (a) Image of the microfluidic spray nozzle in operation. The device has two inlets: one for the compressed gas and one for the solution (protein mixture) to be nebulised. (b) Schematic representation of the flow splitter. The splitter has two calibrated capillaries determining the fraction of the total flow incoming from LC separation directed to the spray nozzle and the fractionation outlet. The flow Q_1 through the spray nozzle is monitored with a flow sensor. (C) QCM mass deposition calibration. A 0.4 mg/mL NaCl solution is sprayed at a known flow rate onto the surface of the sensor, which results in a linear frequency decrease trend. This indicates a constant mass deposition rate and a linear frequency response to mass loading for the dry mass of deposits in air.

Quartz Crystal Microbalance

A commercially available 5 MHz resonant frequency QCM crystal (Stanford Research Systems 100RX1, Cr/Au) was used. Crystal resonant frequency monitoring is performed with a frequency counter (Stanford Research Systems QCM200) with a gate time of 1 s, leading to frequency stability of 0.1 Hz in a stabilised environment. The first electrode of the QCM sensor has an area of 1.37 cm^2, however, the active electrode oscillation area is confined to 0.40 cm^2 by the geometry of the second electrode. The Sauerbrey[22] equation can relate the change in the resonant crystal frequency Δf_q to the mass changes on the surface Δm_q:

$$\Delta f_q = \frac{2 f_q^2}{A\sqrt{\rho_q \mu_q}} \Delta m_q \tag{3}$$

were f_q is the resonant frequency of the crystal and ρ_q and μ_q are the density and shear modulus of quartz, respectively, giving the mass sensitivity coefficient $\Delta f / \Delta m = 0.1415$ Hz/ng.

Results and discussion

Inline spray control

LC separation typically operates at 0.01-1 mL/min flow while an average microfluidic device flow is around 1-10 µL/min presenting a mismatch over a few orders of magnitude. In this section, we explain how we use a flow splitter to couple the two systems.

The total flow incoming to the splitter was varied between 1300 µL/h and 1800 µL/h and measured at the spray nozzle (Supplementary Figure 1a), showing a direct correlation between the LC and the spray flow rates. By plotting the flow through the spray nozzle versus the total flow a linear relationship was obtained (Supplementary Figure 1b). The least square fit yields an estimate to the gradient m=$R_2/(R_1 + R_2)$ = (0.7578 ± 0.0006) and the intercept c=$-P_S/(R_1 + R_2)$ = -967 ± 1 µL/h . We can thus observe a difference of these values with respect to the expected parameters for the gradient and intercept of m = 0.38 and c = -740 µL/h which were estimated in the methods section. This discrepancy occurs due to the fact that at high pressures PDMS deforms, thus expanding the nozzle liquid channel, and subsequently significantly reducing the on chip resistance. Assuming that the PEEK capillary resistance, R_2, does not change we obtain a value for the spray inlet hydraulic resistance to be $R_1 = 1.8 \cdot 10^{14}$ Pa·s/m^3 which is about 5 times smaller than expected value, indicating a significant channel cross-sectional area expansion. Hydraulic resistance has a strong dependency on the hydraulic channel diameter, $R_{res} \propto 1/(D_{hyd})^4$. Therefore, we can estimate that the spray inlet channel hydraulic diameter increased by 50% due to the additional pressure ($1.5^4 \approx 5$). Using the corrected R_1 value we estimate the pressure at the nozzle orifice to be $P_S = 2$ bar showing that there is about 1 bar gas pressure drop along the gas flow path on chip. Overall, we have established a predictable linear flow splitting performance. Nevertheless, the flow to the spray nozzle during all the experiments was still monitored, as slight device-to-device variation can affect the P_S value. In order to avoid such a discrepancy, glass micro-devices could be fabricated, thus allowing

for more robust microchannels to further optimize the spray system performance.

Calibration and sensitivity evaluation

QCM sensors are known to have a complex frequency response as a function of mass loading in solution.[17] However, in our case, a uniform layer of analytes could be deposited onto the sensor surface, which creates a linear sensor response. This was verified by spraying a 0.4 mg/mL NaCl buffer solution at a constant rate while observing the sensor frequency change as shown in Figure 2C. We observed a linear frequency decrease trend with a gradient of -1.3015 ± 0.0006 Hz/s which gives a mass deposition rate of 9.2 ± 0.004 ng/s when using frequency to mass relationship (see Methods). The flow through the spray nozzle is measured to be Q_s = 141.5 ± 8.4 µL/h, thus, the expected mass deposition rate is 15.7 ± 0.93 ng/s. Taking the ratio of the two, we obtain the calibration factor of 58.5 ± 3.5 % which reflects the fact that not all of the mass deposited on the sensor, lands on the sensitive overlapping QCM electrode area, due to the angle of the spray.

Separation and desalting

While in molecular biology and protein separation approaches, buffers are commonly used to stabilise and maintain the activity and structure of proteins, such buffers are composed from a wide range of salt compositions. Such salt-rich solutions might reduce the sensitivity towards the dry mass of the proteins themselves, thus we have integrated a desalting step to increase the sensitivity of measurements.

We first separated the individual proteins thyroglobulin, aldolase and ovalbumin, which are in a mixture (all protein concentration 1 mg/mL) at a flow rate of 26 µL/min (Figure 3a). The flow between volumes 0.9 mL and 1.3 ml was then bypassed, and the purified thyroglobulin solution was injected into a water prefilled desalting column. The specific protein fraction is first desalted and subsequently eluted from the desalting column between 1.1 mL and 2 mL of the desalting volume following the flow bypass. We further confirmed

that the buffer salts are delayed by the desalting column with a conductivity measurement using AKTA Pure conductivity detector (Figure 3b). The purified and desalted protein solution was then injected into the flow splitter resulting in a flow through the device of $Q_s = 215.2 \pm 9.5$ µL/h giving a ratio of 13.8 ± 0.61 % of the total sample being spray dried onto the QCM and about 86 % of the total sample fractionated. As expected, we observed a rapid QCM resonant frequency decrease due to the protein deposited on the sensor surface as explained in the previous section, followed by a gradual deposition of the buffer salts (Figure 3c). We measured the frequency shift between 1.1 mL and 2 mL volume points to be 488 ± 33 Hz indicating a detected protein mass of 3.45 ± 0.23 µg.

Label-free Thyroglobulin detection

Next, we explored the concentration dependence of the selective protein detection method presented in this study. Four protein solutions with thyroglobulin concentrations ranging between 0.5 mg/mL to 2 mg/mL were prepared. The desalted protein peak deposited on the QCM caused a frequency decrease of 264 ± 51 Hz, 488 ± 33 Hz, 700 ± 29 Hz and 875 ± 38 Hz for thyroglobulin concentrations of 0.5, 1, 1.5 and 2 mg/mL, respectively (Figure 5a). The frequency shifts correspond to the detected dry mass of protein landing on the sensitive QCM sensor area 1.87 ± 0.36 µg, 3.45 ± 0.23 µg, 4.95 ± 0.20 µg and 6.19 ± 0.27 µg, respectively. All error bounds were determined by quantifying QCM resonant frequency fluctuations over time.

To estimate the predicted protein mass landing on the sensor surface we consider the total mass within the 40 µL injected sample volume and multiply it by the previously obtained 0.138 ± 0.006 flow splitting ratio and a fraction of 0.585 ± 0.035 landing on the sensitive QCM area. Thus, the expected proportion of the total injected protein sample is 8.1 ± 0.6 % giving a gradient of 3.23 ± 0.24 µL in the detected mass versus the protein concentration plot as shown in Figure 5b. We can conclude that the measured protein masses are in good agreement with the predicted protein amounts.

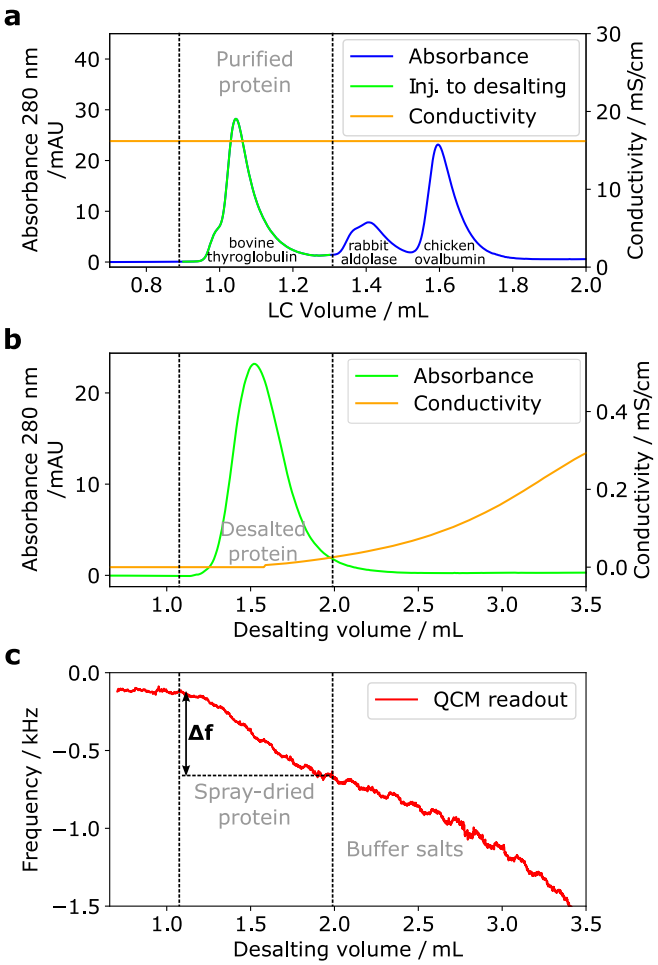

Figure 3: Protein separation and desalting. (a) The thyroglobulin, aldolase and ovalbumin mixture is separated on the LC column in PBS buffer. (b) A well separated thyroglobulin peak is selected and injected into a protein desalting column. The buffer salts are delayed as expected, resulting in a gradual conductivity increase. (c) We finally deposit the desalted protein solution onto a gravimetric QCM sensor showing a non-linear mass deposition rate. The first frequency jump is caused by the desalted protein and a subsequent rapid frequency decrease trend due to the delayed buffer salt deposition.

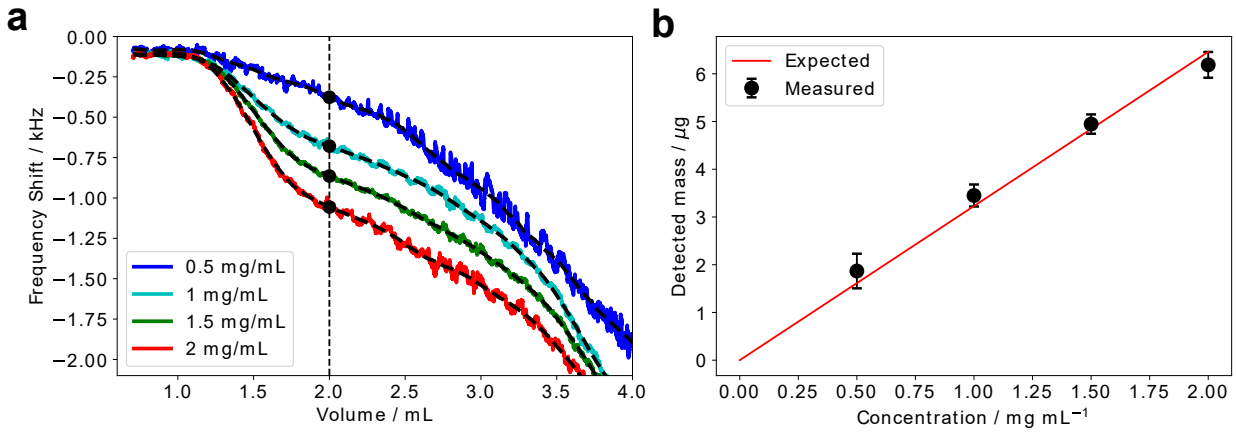

Figure 4: Selective label-free gravimetric thyroglobulin detection. (a) QCM frequency decrease due to the desalted thyroglobulin deposition is dependent on the initial protein concentration within the mixture. (b) The mass detected by the QCM as a function of the injected protein concentration is in agreement with the predicted mass quantity taking into account the previously evaluated split ratio and the QCM-spray calibration.

Limits of detection

Finally, we quantified the limit of detection (LOD) of our approach, by estimating the variation of the amount of evaporating deionised water droplets on the sensor surface, leaving no residue. We measured the standard deviation of frequency fluctuations compared to a smoothed frequency trend and obtained a standard deviation of around $f_{noise} = 30$ Hz. Since the frequency change is measured by taking the difference between two points, each with an error of 30 Hz, the total error in the difference is $30\sqrt{2} \approx 42$ Hz which corresponds to the minimum measurable mass of 0.3 µg. By combining this value with the protein calibration constants obtained above, we estimate the smallest reliably detectable protein concentration presented in this study to be 100 µg/mL, which is mainly related to continuous evaporation of water droplets on the sensor surface.

Finally, the successful implementation of the method presented in this manuscript relies upon the performance of a desalting column and introduces a lower bound of system LOD. Buffer conductivity at an elution volume of 2 ml was a approximately 0.02 mS/cm (Figure 3b). Assuming a linear correlation between the buffer conductivity and salt mass concen-

tration, we estimate the concentration of buffer salt to be 12.5 ug/ml. The conductivity of the buffer is increasing in an approximately linear fashion between elution volumes of 1.6-2 ml, hence, the effective salt mass concentration in the sample mixed with the protein can be estimated to be 3 μg/mL. This LOD limit of the system is based on desalting column performance and can be further improved upon.

Conclusions

The label-free detection of proteins in complex mixtures is key to advancing our understanding of protein interactions with other biomolecules under physiological conditions. However, commonly used bulk analytical approaches present limitation in the ability to separate individual protein species and their characterisation in a label-free manner, thus requiring additional time consuming steps. This work presents an approach for overcoming these challenges by performing an integrated selective label-free protein sensing through coupling liquid chromatography with a gravimetric QCM detection via a microfluidic spray nozzle, resulting in protein mass detection limits at the microgram level. To this effect, a standard protein mixture containing three model proteins, thyroglobulin, aldolase and ovalbumin, was separated using LC, immediately followed by a desalting step to allow for the integration of chromatography with a microfluidic spray gravimetric analysis of thyroglobulin as a target. By spraying a buffer solution, we verified that the mass detection principle is linear with respect to mass loading and then demonstrated that the measurement is quantitative by varying the thyroglobulin concentration within the mixture. The devised analysis approach only requires the consumption of 14% of the total fractionated volume for gravimetric QCM analysis, thus allowing for the remaining 86 % of the sample to be utilised for further experimental procedures. Moreover, by improving on the desalting performance and gating the spray deposition time followed by sensor equilibration, the minimally detectable frequency shift is approximately 0.1 Hz leading to a 1 µg/mL detection level. These results therefore

suggest that the sensing approach presented here can be integrated with a wide variety of acoustic gravimetric sensors, thus opening the possibility of new opportunities for a selective, low concentration, label-free protein detection.

Acknowledgements

The research presented in this manuscript has received funding from the European Research Council under the European Union's Seventh Framework Programme (FP7/2007-2013) through the ERC grant PhysProt (agreement no. 337969). We gratefully acknowledge financial support from the Engineering and Physical Sciences Research Council (EPSRC) (TPJK), the Frances and Augustus Newman Foundation (TPJK) and the Oppenheimer Early Career Fellowship (AL). We also acknowledge support from the Nanotechnologies Doctoral Training Centre in Cambridge (NanoDTC Cambridge EP/L015978/1) (TK). We further thank Fluidic Analytics LtD for the collaboration and continued support for the project.

Supporting Information for Publication

Supporting Figure 1 - Plots showing flow splitter performance and calibration.

Conflict of interests

The authors declare that they have no conflict of interest.

References

(1) Vollmer, F.; Arnold, S. Whispering-gallery-mode biosensing: label-free detection down to single molecules. *Nat. Methods* **2008**, *5*, 591.

(2) Jones, S.; Thornton, J. M. Principles of protein-protein interactions. *Proc. Natl. Acad. Sci. U.S.A.* **1996**, *93*, 13–20.

(3) Aguzzi, A.; O'connor, T. Protein aggregation diseases: pathogenicity and therapeutic perspectives. *Nat. Rev. Drug Discov.* **2010**, *9*, 237.

(4) Star, A.; Tu, E.; Niemann, J.; Gabriel, J.-C. P.; Joiner, C. S.; Valcke, C. Label-free detection of DNA hybridization using carbon nanotube network field-effect transistors. *Proc. Natl. Acad. Sci. U.S.A.* **2006**, *103*, 921–926.

(5) Xiao, Y.; Lubin, A. A.; Heeger, A. J.; Plaxco, K. W. Label-free electronic detection of thrombin in blood serum by using an aptamer-based sensor. *Angew. Chem. Int. Ed. Engl.* **2005**, *117*, 5592–5595.

(6) Toprakcioglu, Z.; Challa, P.; Xu, C.; P. J. Knowles, T. Label-Free Analysis of Protein Aggregation and Phase Behavior. *ACS Nano* **2019**, *13*, 13940–13948.

(7) Young, G. et al. Quantitative mass imaging of single biological macromolecules. *Science* **2018**, *360*, 423–427.

(8) Vashist, S. K.; Schneider, E. M.; Luong, J. H. Commercial smartphone-based devices and smart applications for personalized healthcare monitoring and management. *Diagnostics* **2014**, *4*, 104–128.

(9) Weile, J.; Knabbe, C. Current applications and future trends of molecular diagnostics in clinical bacteriology. *Anal. Bioanal. Chem.* **2009**, *394*, 731–742.

(10) Longo, G.; Alonso-Sarduy, L.; Rio, L. M.; Bizzini, A.; Trampuz, A.; Notz, J.; Dietler, G.; Kasas, S. Rapid detection of bacterial resistance to antibiotics using AFM cantilevers as nanomechanical sensors. *Nat. nanotechnol.* **2013**, *8*, 522.

(11) Otzen, D. Functional amyloid: turning swords into plowshares. *Prion* **2010**, *4*, 256–264.

(12) Hol, F. J.; Dekker, C. Zooming in to see the bigger picture: microfluidic and nanofabrication tools to study bacteria. *Science* **2014**, *346*, 1251821.

(13) Wang, W. U.; Chen, C.; Lin, K.-h.; Fang, Y.; Lieber, C. M. Label-free detection of small-molecule–protein interactions by using nanowire nanosensors. *Proc. Natl. Acad. Sci. U.S.A.* **2005**, *102*, 3208–3212.

(14) Yang, Y.-T.; Callegari, C.; Feng, X.; Ekinci, K. L.; Roukes, M. L. Zeptogram-scale nanomechanical mass sensing. *Nano lett.* **2006**, *6*, 583–586.

(15) Arlett, J.; Myers, E.; Roukes, M. Comparative advantages of mechanical biosensors. *Nat. nanotechnol.* **2011**, *6*, 203.

(16) Lucklum, R.; Hauptmann, P. Acoustic microsensors—the challenge behind microgravimetry. *Anal. Bioanal. Chem.* **2006**, *384*, 667–682.

(17) Dufour, I.; Lemaire, E.; Caillard, B.; Debéda, H.; Lucat, C.; Heinrich, S. M.; Josse, F.; Brand, O. Effect of hydrodynamic force on microcantilever vibrations: Applications to liquid-phase chemical sensing. *Sens. Actuators B Chem.* **2014**, *192*, 664–672.

(18) Vančura, C.; Dufour, I.; Heinrich, S. M.; Josse, F.; Hierlemann, A. Analysis of resonating microcantilevers operating in a viscous liquid environment. *Sens. Actuator A Phys.* **2008**, *141*, 43–51.

(19) Waggoner, P. S.; Tan, C. P.; Bellan, L.; Craighead, H. G. High-Q, in-plane modes of nanomechanical resonators operated in air. *J. Appl. Phys.* **2009**, *105*, 094315.

(20) Onen, O.; Ahmad, A. A.; Guldiken, R.; Gallant, N. D. Surface modification on acoustic wave biosensors for enhanced specificity. *Sensors* **2012**, *12*, 12317–12328.

(21) White, D. A.; Buell, A. K.; Dobson, C. M.; Welland, M. E.; Knowles, T. P. Biosensor-based label-free assays of amyloid growth. *FEBS Lett.* **2009**, *583*, 2587 – 2592.

(22) Sauerbrey, G. Verwendung von Schwingquarzen zur Wägung dünner Schichten und zur Mikrowägung. *Z. phys.* **1959**, *155*, 206–222.

(23) Hlavay, J.; Guilbault, G. Applications of the piezoelectric crystal detector in analytical chemistry. *Anal. Chem.* **1977**, *49*, 1890–1898.

(24) Kanazawa, K. K.; Gordon II, J. G. The oscillation frequency of a quartz resonator in contact with liquid. *Anal. Chim. Acta.* **1985**, *175*, 99–105.

(25) Rickert, J.; Brecht, A.; Göpel, W. QCM operation in liquids: constant sensitivity during formation of extended protein multilayers by affinity. *Anal. Chem.* **1997**, *69*, 1441–1448.

(26) Knowles, T. P.; Shu, W.; Devlin, G. L.; Meehan, S.; Auer, S.; Dobson, C. M.; Welland, M. E. Kinetics and thermodynamics of amyloid formation from direct measurements of fluctuations in fibril mass. *Proc. Natl. Acad. Sci. U.S.A.* **2007**, *104*, 10016–10021.

(27) Godber, B.; Frogley, M.; Rehak, M.; Sleptsov, A.; Thompson, K. S.; Uludag, Y.; Cooper, M. A. Profiling of molecular interactions in real time using acoustic detection. *Biosens. Bioelectron.* **2007**, *22*, 2382–2386.

(28) Doy, N.; McHale, G.; Newton, M.; Hardacre, C.; Ge, R.; MacInnes, J.; Kuvshinov, D.; Allen, R. Small volume laboratory on a chip measurements incorporating the quartz crystal microbalance to measure the viscosity-density product of room temperature ionic liquids. *Biomicrofluidics* **2010**, *4*, 014107.

(29) Burg, T. P.; Godin, M.; Knudsen, S. M.; Shen, W.; Carlson, G.; Foster, J. S.; Babcock, K.; Manalis, S. R. Weighing of biomolecules, single cells and single nanoparticles in fluid. *Nature* **2007**, *446*, 1066.

(30) Modena, M. M.; Wang, Y.; Riedel, D.; Burg, T. P. Resolution enhancement of sus-

pended microchannel resonators for weighing of biomolecular complexes in solution. *Lab Chip* **2014**, *14*, 342–350.

(31) Olcum, S.; Cermak, N.; Wasserman, S. C.; Manalis, S. R. High-speed multiple-mode mass-sensing resolves dynamic nanoscale mass distributions. *Nat. Commun.* **2015**, *6*, 7070.

(32) Reviakine, I.; Johannsmann, D.; Richter, R. P. Hearing What You Cannot See and Visualizing What You Hear: Interpreting Quartz Crystal Microbalance Data from Solvated Interfaces. *Anal. Chem.* **2011**, *83*, 8838–8848, PMID: 21939220.

(33) Müller, T.; White, D.; Knowles, T. Dry-mass sensing for microfluidics. *Appl. Phys. Lett.* **2014**, *105*, 214101.

(34) Kartanas, T.; Ostanin, V.; Challa, P. K.; Daly, R.; Charmet, J.; Knowles, T. P. Enhanced Quality Factor Label-free Biosensing with Micro-Cantilevers Integrated into Microfluidic Systems. *Anal. Chem.* **2017**, *89*, 11929–11936.

(35) Chan, B.-D.; Icoz, K.; Huang, W.; Chang, C.-L.; Savran, C. A. On-demand weighing of single dry biological particles over a 5-order-of-magnitude dynamic range. *Lab Chip* **2014**, *14*, 4188–4196.

(36) Lazcka, O.; Del Campo, F. J.; Munoz, F. X. Pathogen detection: A perspective of traditional methods and biosensors. *Biosens. Bioelectron.* **2007**, *22*, 1205–1217.

(37) Bhunia, A. K. *Advances in food and nutrition research*; Elsevier, 2008; Vol. 54; pp 1–44.

(38) Harrison, D. J.; Manz, A.; Fan, Z.; Luedi, H.; Widmer, H. M. Capillary electrophoresis and sample injection systems integrated on a planar glass chip. *Anal. Chem.* **1992**, *64*, 1926–1932.

(39) Snyder, L. R.; Kirkland, J. J.; Dolan, J. W. *Introduction to modern liquid chromatography*; John Wiley & Sons, 2011.

(40) Turgeon, R. T.; Bowser, M. T. Micro free-flow electrophoresis: theory and applications. *Anal. Bioanal. Chem.* **2009**, *394*, 187–198.

(41) Mori, S.; Barth, H. G. *Size exclusion chromatography*; Springer Science & Business Media, 2013.

(42) Tamaoka, J.; Komagata, K. Determination of DNA base composition by reversed-phase high-performance liquid chromatography. *FEMS Microbiol. Lett.* **1984**, *25*, 125–128.

(43) Jungbauer, A.; Hahn, R. *Methods in enzymology*; Elsevier, 2009; Vol. 463; pp 349–371.

(44) Cuatrecasas, P. Protein purification by affinity chromatography derivatizations of agarose and polyacrylamide beads. *J. Biol. Chem.* **1970**, *245*, 3059–3065.

(45) Amstad, E.; Spaepen, F.; Brenner, M. P.; Weitz, D. A. The microfluidic nebulator: production of sub-micrometer sized airborne drops. *Lab Chip* **2017**, *17*, 1475–1480.

(46) Ficarro, S. B.; Salomon, A. R.; Brill, L. M.; Mason, D. E.; Stettler-Gill, M.; Brock, A.; Peters, E. C. Automated immobilized metal affinity chromatography/nano-liquid chromatography/electrospray ionization mass spectrometry platform for profiling protein phosphorylation sites. *Rapid Commun. Mass Spectrom.* **2005**, *19*, 57–71.

(47) Scheidt, T.; Kartanas, T.; Peter, Q.; Schneider, M. M.; Saar, K. L.; Müller, T.; Challa, P. K.; Levin, A.; Devenish, S.; Knowles, T. P. J. Multidimensional protein characterisation using microfluidic post-column analysis. *Lab Chip* **2020**, –.

(48) Challa, P. K.; Kartanas, T.; Charmet, J.; Knowles, T. P. Microfluidic devices fabricated using fast wafer-scale LED-lithography patterning. *Biomicrofluidics* **2017**, *11*, 014113.

(49) Kartanas, T.; Toprakcioglu, Z.; Hakala, T. A.; Levin, A.; Herling, T. W.; Daly, R.; Charmet, J.; Knowles, T. P. Mechanism of droplet-formation in a supersonic microfluidic spray device. *Appl. Phys. Lett.* **2020**, *116*, 153702.

(50) Toprakcioglu, Z.; Levin, A.; Knowles, T. P. J. Hierarchical Biomolecular Emulsions Using 3-D Microfluidics with Uniform Surface Chemistry. *Biomacromolecules* **2017**, *18*, 3642–3651.

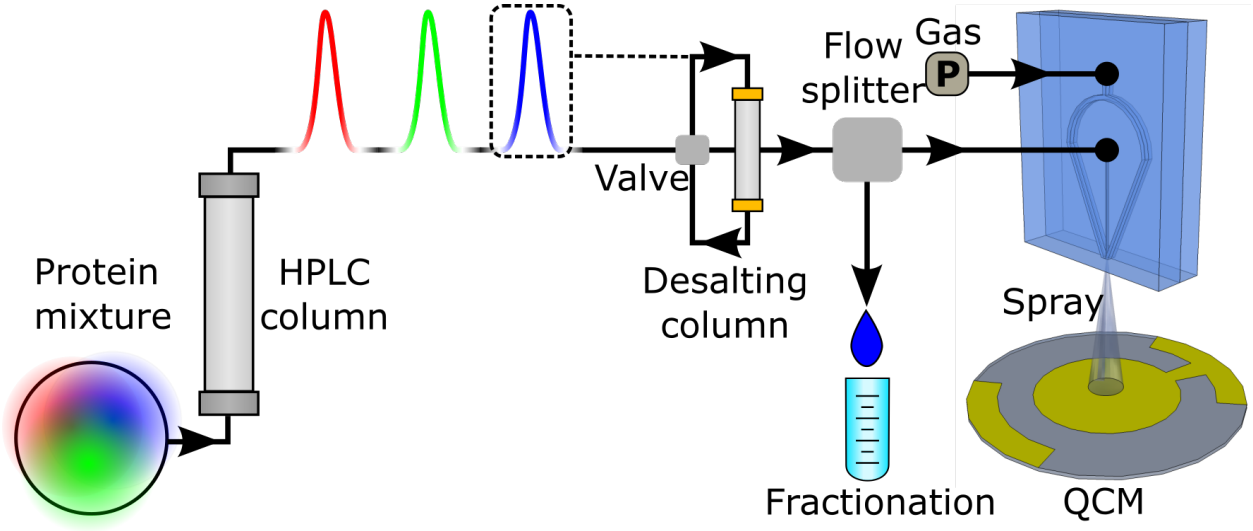

Figure 5: Graphic Table of Content.